Membrane compaction in Forward Osmosis Process

Daniel Yee Fan Ng[1,2], Yunfeng Chen[1], Zhili Dong[3], Rong Wang[1,4*]

1. Singapore Membrane Technology Centre, Nanyang Environment and Water Research Institute, Nanyang Technological University, 1 Cleantech Loop, CleanTech One #06-08, Singapore 637141

2. Interdisciplinary Graduate School, Nanyang Technological University, 50 Nanyang Avenue, Singapore 639798

3. School of Material Science and Engineering, Nanyang Technological University, 50 Nanyang Avenue, Singapore 639798

4. School of Civil and Environmental Engineering, Nanyang Technological University, 50 Nanyang Avenue, Singapore 639798

[*]Corresponding author:

Rong Wang, rwang@ntu.edu.sg

Phone: 65-67905327

Abstract

Membrane compaction is commonly observed in polymeric membranes when subjected to elevated hydraulic pressure, but was rarely discussed in forward osmosis (FO) processes, since there was usually little hydraulic pressure difference across the membrane. In the current study, three TFC membranes were fabricated using hollow fiber substrates with varied water permeability to study the effect of the osmotic pressure on the TFC membranes. The TFC membranes were continuously tested in FO experiments for 24 hours by using DI water as feed and NaCl solutions of different concentrations as draw solution, and their performances were checked again using fresh feed solutions. At the end of FO experiments, all TFC membranes experienced water flux and salt flux decline to different extents. The TFC membranes were characterized using SEM, TEM and AFM. Visible changes in the cross-section morphology and surface topography of the TFC membranes were observed after FO experiments. The observation suggested that the occurrence of membrane compaction could be associated with "negative pressure" build-up within the support layer of the TFC membranes. The current study could shed light on the important factors that should be considered during membrane fabrication and when establishing the testing protocols for the characterization of FO membrane.

Key words: forward osmosis (FO) process; membrane compaction; mass transfer resistance of support layer; membrane characterization; long-term operation.

Graphical abstract

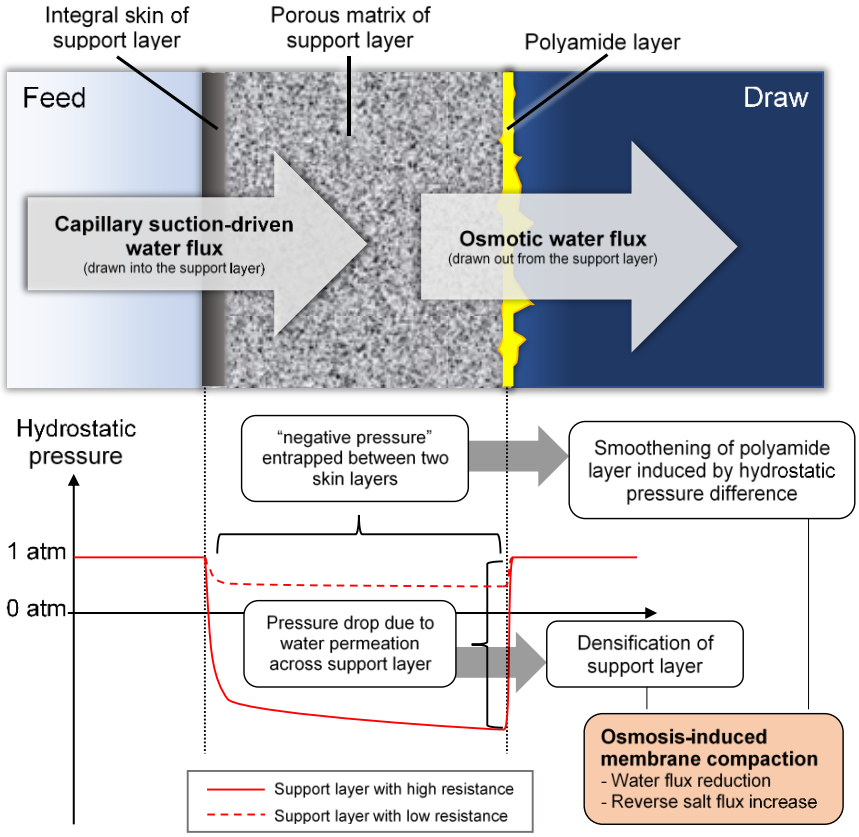

1. Introduction

Engineered osmosis process has received much attention as the alternative technology with no/low external energy consumption, in comparison to hydraulic pressure-driven membrane separation processes. Forward osmosis (FO) involves the use of a semi-permeable membrane to establish preferential movement of solvent molecules from a solution of low osmotic pressure (feed solution) into another solution with higher osmotic pressure (draw solution). Due to the difference in chemical potential energy between the two solutions, spontaneous permeation of solvent across the membrane is favoured in nature. Therefore, the energy consumption of FO process itself is very low as compared to other membrane processes. As such, it has been proposed to couple FO with other hydraulic pressure-driven or thermal-driven membrane processes to produce potable water with reduced overall energy consumption and lower membrane fouling potential [1, 2].

Being the heart of FO process, the characteristics of the semi-permeable membrane could dominate the feasibility of adapting it to specific applications. A desired FO membrane should possess with a highly porous substrate to mitigate the internal concentration polarization (ICP) and a dense selective layer that can reject solutes effectively. Thin-film composite (TFC) membranes is one of the most common types of membrane structure applied in FO-related studies. It is typically fabricated by interfacial polymerization technique, forming an ultrathin and highly crosslinked selective layer on the surface of porous ultrafiltration (UF) substrate [3].

Despite that FO membranes with high water flux and low reverse salt flux have been developed over recent years [4, 5], there are concerns on the sustainability of membrane performance in long term operation. It has been observed that FO membranes were more resistant to fouling when they were operated in active-layer-facing-feed-solution (AL-FS) configuration [6-10]. However, this membrane orientation could suffer significant loss in the osmotic driving force due to severe dilutive ICP, hence leading to inherently low water flux. In contrast, when the membrane is operated in active-layer-facing-draw-solution (AL-DS) configuration, since the active layer is in direct contact with the draw solution, the influence of ICP is rather minor and a greater portion of osmotic driving force could be utilized. Yet, organic foulants and scaling precursors from feed solution could easily penetrate into the support layer of FO membranes in AL-DS configuration. The deposition and accumulation of foulants inside the porous support layer could lead to significant reduction in water flux due to increased membrane resistance and enhanced ICP [6, 8]. The trapped foulants in the substrate are difficult to be removed due

to the lack of hydrodynamic shear force within the support layer, hence making the membrane fouling in the AL-DS orientation highly irreversible [11]. As such, double-skinned membranes has been proposed as the solution which could potentially mitigate membrane fouling, and at the same time improve the utilization of osmotic driving force by minimizing ICP within the membrane [12-17].

On the other hand, it is well recognized that the mechanical stability of membranes is important to ensure membrane's long-term operation. For hydraulic pressure-driven membrane processes, polymeric membranes could experience certain degree of densification under the stress induced by applied pressure, leading to gradual increase in mass transfer resistance and thus decrease in membrane permeability over time. Such phenomena is known as compaction, and it could significantly reduce the flux of reverse osmosis (RO), nanofiltration (NF) and UF as well as gas separation membranes over the early stage of operation [18, 19]. Under certain circumstances, compaction could contribute to flux reduction of up to 60% of initial flux [18]. Many attempts were made to increase the mechanical stability of membranes in order to improve their resistance to compaction [20, 21]. In RO process, membrane compaction could reduce the water permeability coefficient of the membrane, and the effect is more significant with elevated pressure and temperature [22]. Compaction of RO membranes could be partially reversible as well, where water permeability coefficient increased with reducing pressure [23, 24]. It was also shown that the severity of membrane compaction was affected by the surface roughness of the membrane [24]. Other studies also suggested that membrane compaction could induce significant increase in the resistance of the porous support layer of the TFC membranes, which may contribute substantially to the overall resistance of the membranes [25].

Compaction of polymeric membranes is influenced by time-dependent phenomena such as plasticisation, swelling and creep of the polymer [26-29]. Attempts have been made to correlate compaction behaviour of the membrane to the physical characteristic of the membrane by using viscoelastic models [18, 30], which predicted the flux decline better than the traditional power law relation. Although the compaction may take place slowly over long time of operation, the lack of proper assessment on the contribution of compaction on membrane performance could significantly interfere with the results of lab-scale studies [18]. Pre-compaction is the typical solution that were applied to isolate the influence of compaction and decoupled it from other factors that could affect membrane performance. Still, the duration of pre-compaction process, which is appropriate to achieve a relatively stable performance, could vary significantly with

the type of membranes. Even for the same type of commercial membrane, the adequate duration of pre-compaction could be very different [31, 32].

On the other hand, it was noted that little attention was paid to membrane compaction during FO operation and the possible influence of compaction on the performance of FO membranes in long term operations. In most situations, there is no external hydraulic pressure applied in FO process. Thus, it was commonly presumed that there is no significant stress exerted on the membrane. Also, the characterization of intrinsic FO performance of membranes was mostly carried out through short-duration experiments in the lab studies (<2 hours) [33, 34], where the reduction of effective osmotic gradient due to dilution of draw solution and draw solute accumulation in feed solution was normally not examined thoroughly. However, in our recent lab study, it was observed that the water flux of FO membranes decreased gradually when it was tested in the AL-DS orientation over 24 hours. The flux decline was more significant for the double-skinned FO membrane tested by using high concentration draw solution. We wondered if there was time-dependent transformation in membrane structure, i.e., membrane compaction that could also occur on the FO membrane process, which might have been ignored in short-duration experiments.

In order to confirm this phenomenon, understand the mechanism behind and investigate its influence on the membrane performance in FO process, three types of hollow fiber TFC membranes, including one with single-layered substrate and two with dual-layered substrates were specially designed and fabricated. The FO performance of the membranes were characterized by using draw solutions with different concentrations and their water and salt flux patterns over time were compared to elucidate the possible connections between the compaction behaviour of TFC membranes and the mass transfer resistance of support layer, as well as the osmotic driving force presented across the membranes. Changes in membrane morphology, surface topography and structure during FO experiments were also analysed through the inspection of the tested membranes under scanning electron microscope (SEM), transmission electron microscope (TEM) and atomic force microscope (AFM). The possible causes of compaction in FO process were proposed based on the experimental observations of TFC membranes. It is envisaged that this study could shed light on the important factors that should be taken into account during FO membrane fabrication and when establishing testing protocols for the characterization of FO membrane.

2. Experimental

2.1 Materials

For the preparation of polymer dope solutions, Veradel® 3000P Polyethersulfone (PES) was supplied by Solvay Advanced Polymers; N-methyl-2-pyrrolidone (NMP), polyethylene glycol 200 (PEG, Mw = 200 g/mo) and acetone (Ac) were purchased from Merck Chemicals; while polyvinylpyrrolidone (PVP, Mw = 1,300,000 g/mol) was purchased from Acros Organics. Glycerol (85%) was obtained from Merck Chemicals for post-treatment of hollow fiber substrates. Cyclohexane, 1,3,5-benzenetricarbonyl trichloride (TMC) and m-phenylenediamine (MPD) were purchased from Sigma-Aldrich and used in the fabrication of TFC membrane. Dextran of various molecular weights were purchased from Sigma-Aldrich and used in crossflow filtration experiments for determination of molecular weight cut-off (MWCO) of the hollow fiber substrates. Sodium chloride (NaCl) was supplied from Merck Chemicals and used for the characterization of TFC membrane intrinsic properties and FO performances. Deionized (DI) water was used to prepare all aqueous solutions in this study, which was produced by Milli-Q system (Millipore, USA).

2.2 Hollow fiber membrane fabrication

2.2.1 Substrates and module preparation

Hollow fiber membranes which were used as the substrate for the preparation of TFC membranes were fabricated via non-solvent induced phase separation (NIPS) technique [35, 36]. The fabrication process of hollow fiber substrate is schematically illustrated in **Figure 1**. In order to produce hollow fiber substrates with highly asymmetric structures, co-extrusion method [35, 37] was employed through the use of a triple-channel spinneret during hollow fiber spinning process. Single-layer hollow fiber substrate denoted as “SL” was fabricated from a dope with lower concentration of polymer and high concentration of pore forming additive (PEG 200), which was extruded through the inner dope channel to form a highly porous structures upon phase inversion.

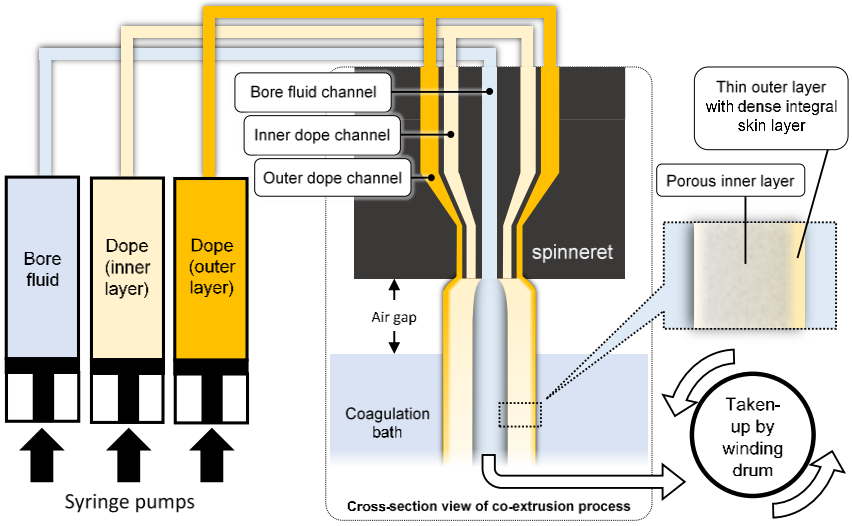

Figure 1. Fabrication of hollow fiber substrates by NIPS process with co-extrusion method.

Based on the spinning condition of SL substrate, dual-layer hollow fiber substrates denoted as "DL#1" and "DL#2" were fabricated by co-extruding an additional layer of dope solution of different composition through the outer dope channel. The additional layer of dope wraps around the shell side (outer surface) of the dope extruded from the inner dope channel. As the result, the two streams of extruded dopes fused and underwent phase inversion together to form an integral structure. Since the dopes with higher polymer concentration were extruded through the outer dope channel at a relatively low flow rate as compared to the dope extruded through the inner dope channel, a much thinner but denser integral skin layer was formed on the shell side of the dual-layer hollow fiber substrates. All the spinning conditions for hollow fiber substrate fabrication are listed in **Table 1**. Finally, the hollow fiber substrates were stored in tap water and periodically rinsed with fresh tap water for at least three days before they were characterized.

Table 1. Hollow fiber substrate spinning conditions.

Hollow fiber substrate	**SL**	**DL#1**	**DL#2**
Dope composition (wt%)			
(PES/NMP/PEG/PVP/Ac/H_2O)			
- inner layer	20/40/40/0/0/0	20/40/40/0/0/0	20/40/40/0/0/0
- outer layer	-	29.2/50.3/0/16.8/1.0/2.8	30.0/52.1/0/17.4/0.5/0
Spinneret dimension (μm)			
- bore fluid channel ID	360		
- inner dope channel ID/OD	620/890		
- outer dope channel ID/OD	1230/1420		
Inner dope flow rate (mL/min)	6.70		
Outer dope flow rate (mL/min)	-	0.30	0.30
Bore fluid composition	DI water		
Bore fluid flow rate (mL/min)	10.0		
Take-up speed (cm/s)	18.85		
Air gap (cm)	1.0		
Coagulation bath composition	Tap water		
Coagulation bath temperature (˚C)	22-23		
Room temperature (˚C)	22-24		
Relative humidity (%)	70-71		

Prior to module preparation, the hollow fiber substrates were immersed in glycerol/water (50/50 wt%) mixture for 1 day. Then, the hollow fibers were dried in the air at room temperature for 1 day. The residual glycerol in the hollow fiber substrates served as the pore preserving agent. Five pieces of glycerol preserved membranes were then packed into lab-scale modules by using epoxy resin (Araldite® Rapid). Each module possessed an effective membrane length of around 25 cm with an effective membrane area between 37 cm^2 to 40 cm^2.

2.2.2 TFC membranes

Inner-selective hollow fiber TFC membranes were prepared by interfacial polymerization reaction. The hollow fiber membranes were first impregnated with MPD by filling the lumen of the modules with the aqueous solution for some time. Then, cyclohexane and TMC solutions were sequentially pumped through the lumen of the modules at constant flow rate, during which MPD and TMC reacted and formed a thin layer of polyamide on membrane surface inside the membrane lumen. The TFC membranes were rinsed and immersed in DI water for 1 day before they were characterized.

2.3 Membrane characterization

2.3.1 Intrinsic property of substrate and TFC FO membrane

Digital microscope (Keyence, Japan) was used to characterize the dimension of hollow fiber substrates. At least 12 measurements were taken with different sections of the membranes to obtain the average dimensions of each substrate. Pure water permeability (PWP) of the substrates were characterized via crossflow filtration experiments, where DI water was circulated over the shell side of the hollow fibers at 1.0 bar applied pressure. PWP (L/m^2/h/bar) was calculated by using the following equation:

$$PWP = \frac{m_p}{\rho_w \cdot A_{eff} \cdot \Delta t \cdot \Delta P} \qquad (1)$$

Where m_p represents the mass of permeate collected from lumen side, ρ_w represents the density of water, A_{eff} represents the effective membrane area (which were calculated based on the outer diameter of the substrates), Δt represents the time interval of measurement and ΔP represents the transmembrane pressure. The MWCO of the substrates were also determined by crossflow filtration experiments, where 2000 ppm dextran solutions (a mixtures of dextran standards with molecular weight range from 6 kDa to 650 kDa) was circulated on the shell side of the substrates at 1.0 bar applied pressure. The feed and permeates were analysed on gel permeation chromatography (GPC) instrument equipped with refractive index (RI) detector (Polymer Laboratories-GPC 50 plus system, Agilent, USA). The MWCO of the substrates were calculated based on the rejection towards dextran molecules of different molecular weights, according to the procedures reported elsewhere [38, 39]. The porosity of substrates was calculated by gravimetric method.

2.3.2 TFC membrane

Water permeability coefficient (A, L/m^2/h/bar) of TFC membranes were characterized via crossflow filtration experiments, where DI water was circulated through the lumen of the module at 2.0 bar applied pressure. The calculation of water permeability coefficient applied the same equation as the calculation of PWP for substrates, except that the mass of permeate collected from shell side was used for the calculation, and the effective membrane area was calculated from the inner diameter of the TFC membranes instead. The salt rejection (R_s, %) and solute permeability coefficient (B, LMH) of TFC membranes was characterized via crossflow low-pressure RO experiments. A 500 ppm NaCl solution was used as the feed

solution and circulated on the lumen side of the TFC membranes at 2 bar applied pressure. The conductivity of permeate (collected from the shell side) and feed were measured by using conductivity meter (ULTRAMETER II™, Cole-Parmer). Salt rejection was calculated by using the equation:

$$R_s = 1 - \frac{E_p}{E_f} \qquad (2)$$

where E_p and E_f represent the conductivity of the permeate and feed, respectively. Solute permeability coefficient was calculated from salt rejection by using the equation:

$$B = \frac{m_p}{\rho_w \cdot A_{eff} \cdot \Delta t} \cdot \left(\frac{1 - R_s}{R_s}\right) \qquad (3)$$

2.3.3 Inspection using SEM, AFM and TEM

The cross-section morphology of TFC membrane was examined under field-emission SEM (JSM-7200F, Jeol, Japan). To prepare samples for SEM, wet membranes were frozen and cleaved in liquid nitrogen to expose the fine structures of membrane cross-section. The samples were then freeze-dried overnight and sputter-coated with platinum (20 mA coating current, 45 sec coating time) prior to inspection under SEM (5 kV acceleration voltage).

The surface topography on the lumen side of TFC membranes was characterized by using AFM (Park Systems, Korea). The membranes were freeze-dried overnight prior to characterization under AFM. To expose the polyamide layer on the lumen side of TFC membranes, the membranes were sliced along the axis and mounted flat on sample disks with the aid of double-sided tapes. The topography images of the polyamide layer were obtained under non-contact mode (NCM) with PPP-NCHR cantilever loaded head. The raw images were processed by using XEI program to generate 3D topographic images and calculate the average roughness of membrane surface.

TFC membranes were characterized with JEM-1400Plus Election Microscope at an acceleration voltage of 120 kV. The membranes were embedded in LR White resin before they were cut into sections for TEM inspection, based on modified procedures from Tang et al [40]. Membrane samples were freeze dried overnight and immersed in 100% ethanol for 1 h. Then, samples were sequentially immersed in 50 wt% (1 h), 67 wt% (2 h), 100 wt% (4 h), and another

100 wt% (24 h) LR White resin. The 50 wt% and 67 wt% LR White resin solutions were prepared by diluting fresh LR White resin with ethanol. Finally, the samples were transferred into gelatin capsules filled with 100% LR White resin and cured at 48 ˚C for 4 days. TEM sections (<100 nm thick) were prepared with Leica Ultracut S Ultramicrotome (Leica, Wetzlar, Germany).

2.4 Forward osmosis experiments

A schematic diagram of the experimental setup used for characterizing the FO performance of the TFC membranes is shown in **Figure 2**. All TFC membranes were characterized in the AL-DS configuration. DI water was used as the feed solution, while NaCl solutions with different concentrations were used as draw solution.

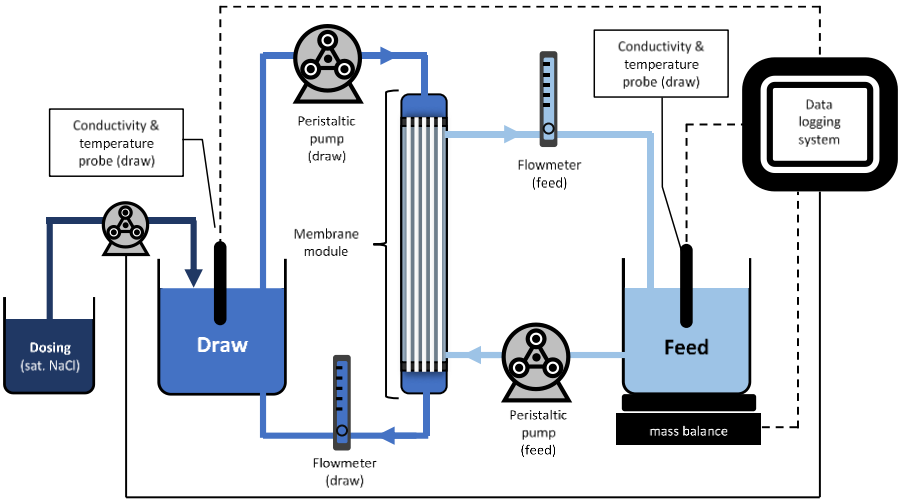

Figure 2. Schematic illustration of forward osmosis experimental setup.

During the FO experiments, feed solution was circulated on the shell side of the membranes at a cross-flow velocity of around 23 cm/s, while draw solution was circulated on the lumen side of the membranes at a cross-flow velocity of around 80 cm/s in counter-current configuration. The temperature of draw and feed solutions were maintained at room temperature (22 – 24 ˚C) throughout the experiments. The conductivity and temperature of draw and feed solutions were monitored by using conductivity probes (Suntex, Taiwan). Dosing pump was used to maintain the concentration of the draw solution based on the conductivity. The mass of the feed solution was monitored by using mass balance (Shimadzu, Japan). The concentration of NaCl in feed and draw solutions were determined based on their conductivity.

The water flux (J_w, L/m^2/h) of the membranes were determined based on the mass change of feed solution (Δm_f) by using the following equation:

$$J_w = \frac{\Delta m_f}{\rho_w \cdot A_m \cdot \Delta t} \qquad (4)$$

where A_m is the effective membrane area based on the inner surface of the hollow fiber. The reverse salt flux ($J_s, g/m^2/h$) of the membranes was determined based on the change in the concentration of NaCl in feed solution (C_f) and the mass of feed solution by using the following equation:

$$J_s = \frac{\Delta(C_f \cdot m_f)}{A_m \cdot \Delta t} \qquad (5)$$

Specific reverse salt flux (J_s/J_w, g/L) was determined by dividing the reverse salt flux with the water flux of the membrane at given time.

In order to investigate the time-dependent process, the FO experiments were carried out under near-ideal conditions for extended duration. To minimize the decrease in osmotic pressure difference between the draw and feed solutions, the concentration of draw solution was maintained by constant dosing with a 5.0 M NaCl solution. Feed solution of relatively large volume (5 – 10 L) was used in each FO test to ensure that the accumulation of draw solute in the feed solution was slowed down significantly. Immediately after the 24-hours FO tests, the final FO performance of each TFC membrane was redetermined by using fresh feed and draw solutions under initial testing conditions to rule out the effect of draw solute accumulation in the feed solution on the membrane performance.

3. Results and Discussion

3.1 Characteristics of membranes

3.1.1 Hollow fiber substrates and TFC membranes

The properties of the hollow fiber substrates fabricated in this study are summarized in **Table 2**. The PWP of the substrates varied significantly with the dope composition changed. The single-layer substrate, denoted as SL, possessed a PWP of 297 L/m^2/h/bar, which was the most permeable among the three substrates fabricated. This was attributed to the use of high concentration of PEG 200, a pore-forming additive which induced the formation of highly

porous skin layer on both shell and lumen sides of SL substrate. The dual-layer substrates, denoted as DL#1 and DL#2, possessed PWP of 16.6 L/m^2/h/bar and 2.83 L/m^2/h/bar, respectively, which were around one and two orders of magnitude lower than the single-layer substrate. Such enormous differences in PWP were contributed by the presence of the relatively thin but significantly less porous layer on the shell side of the dual-layer hollow fiber substrates, which were formed from the dopes containing a higher polymer concentration and very little pore forming additives (see Table 1).

Table 2. Hollow fiber substate properties.

Hollow fiber substrates:	SL	DL#1	DL#2
Dimension (um)			
- inner diameter	900±6	975±27	1013±7
- outer diameter	1185±9	1260±22	1292±7
- thickness	142±4	142±5	140±2
PWP (L/m^2/h/bar)	297±7	16.6±0.5	2.83±0.26
MWCO (kDa)	9.5	1.8	1.9
Porosity (%)	77	78	78

On one hand, all hollow fiber substrates possessed relatively high porosity. The porosities of SL, DL#1 and DL#2 were 77% 78% and 78%, respectively. Despite that much higher polymer concentration was used in the second dope which formed the outer layer of the dual-layer substrates, their overall porosity did not vary substantially from the single-layer substrates. This was ascribed to the higher inner dope flow rate as compared to the outer dope flow rate during membrane fabrication. A large portion of the extruded dope contained high concentration of PEG as the pore forming agent, which formed the thicker but highly porous inner layer. The dope with a higher polymer concentration and very little pore forming agent was extruded at significantly low flow rate to create an extremely thin but dense outer layer. As such, a highly asymmetric hollow fiber membrane with a critically densified top layer can be prepared without sacrificing the bulk porosity of the membrane. The porous support of the three substrates could thus be considered similar.

The intrinsic separation properties of the TFC membranes fabricated in this study are summarised in **Table 3**. The water permeability coefficients of TFC membranes prepared from SL, DL#1 and DL#2 substrates were 4.07 L/m^2/h/bar, 2.41 L/m^2/h/bar and 1.38 L/m^2/h/bar, while their NaCl rejections were 97.2%, 96.3% and 91.7%, respectively.

Table 3. Hollow fiber TFC membrane intrinsic properties.

Hollow fiber TFC membrane	SL-TFC	DL#1-TFC	DL#2-TFC
Water permeability coefficient, A (L/m^2/h/bar)	4.07 ± 0.14	2.41 ± 0.24	1.38 ± 0.09
Salt rejection, R_s (%)	97.2 ± 0.1	96.3 ± 0.7	91.7 ± 0.6
Solute permeability coefficient, B (L/m^2/h)	0.18 ± 0.01	0.16 ± 0.02	0.21 ± 0.02

3.2 FO performance of TFC membrane with single-skinned FO membrane

The performances of SL-TFC membrane over 24 hours of FO tests are shown in **Figure 3**, which were normalized with reference to the performance determined in the first 20 minutes. The initial water flux, reverse salt flux and specific reverse salt flux of SL-TFC membrane were 50.4 L/m^2/h, 2.6 g/m^2/h and 0.051 g/L, respectively, when 0.5 M NaCl was used as draw solution. One the other hand, when 2.0 M NaCl was used as draw solution, the initial water flux, reverse salt flux and specific reverse salt flux of SL-TFC membrane were 110.6 L/m^2/h, 9.2 g/m^2/h, and 0.083 g/L, respectively. For both FO tests carried out with 0.5 M NaCl and 2.0 M NaCl as draw solution, the water flux of SL-TFC membrane stabilized within 1 hour after the FO tests began. There was substantial increase in the reverse salt flux of SL-TFC membranes over the first hour of FO test when 0.5 M NaCl was used, which was likely due to the delay of conductivity measurement when the concentration of draw solute in the feed was extremely low.

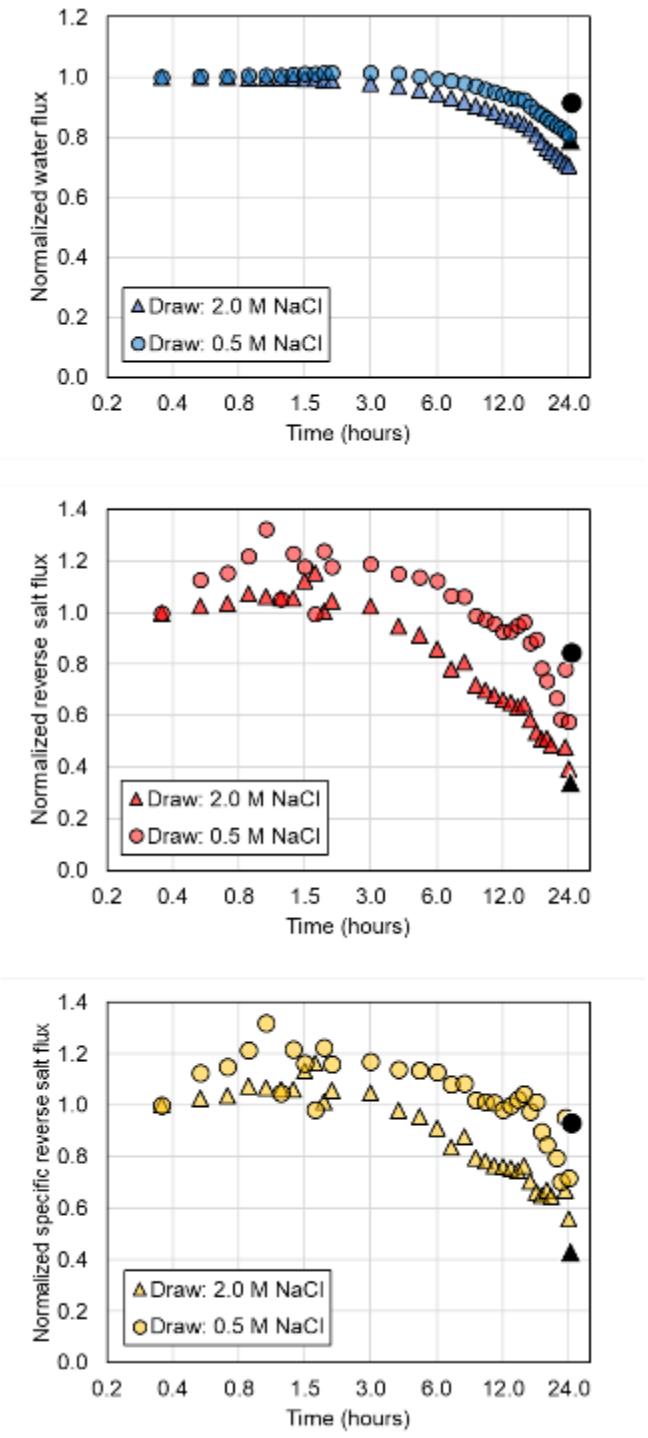

358

359 **Figure 3.** FO performance of SL-TFC membrane characterized by using either 0.5 M NaCl or
360 2.0 M NaCl as draw solution in AL-DS orientation. DI water was used as feed solution. The
361 normalized water flux, normalized reverse salt flux and normalized specific reverse salt flux of
362 the membrane are presented in logarithmic time scale. The final performance of the membrane
363 after 24 hours of experiments are indicated by the bold shaded markers.

364

It can be seen that the water flux and reverse salt flux of SL-TFC membranes tested with draw solution of different concentrations displayed similar patterns over 24 hours of FO test. Both water flux and reverse salt flux of the membrane remained relatively stable over the first 3 hours, but started to decline linearly afterwards until the end of the FO tests. After the 24-hour test, the membrane was re-tested using fresh feed and draw solutions and the results are shown in **Figure 3** (shaded points). It was found that the water flux of the used SL-TFC membrane were 9% and 21% lower, while the reverse salt flux were 16% and 66% lower than the initial values of the fresh membrane, with 0.5 M NaCl and 2.0 M NaCl as draw solutions, respectively. These results indicated that the FO performance of the TFC membrane did not recover completely even after the initial testing conditions were restored. It implied that both the water flux decline and reverse salt flux decline during FO tests were not entirely caused by the changes of feed and draw solutions (such as the accumulation of salt in feed solution due to salt back diffusion). It may suggest that the properties of the support layer changed during FO tests, such that the structural parameter increased, leading to more severe ICP.

In addition, the water flux decline and salt flux decline may also be associated with the decrease in the water permeability and solute permeability of the TFC membrane, which was probably caused by the change of the selective layer. It was also found that the reverse salt flux decreased more significantly than the water flux of SL-TFC membrane, leading to overall reduction in the specific reverse salt flux of 7% and 57% respectively when 0.5M NaCl and 2.0 M NaCl were used as draw solution. Such changes may be interpreted as improvement in membrane selectivity. These results implied that the FO performance that was typically measured through short-duration FO tests may not reflect the stable performance of TFC membranes over a long period of operation, particularly if the osmotic gradient across the membrane is high.

To determine if the reductions in both water flux and salt flux were related to membrane deformation, SL-TFC membranes before and after FO tests were removed from the modules and characterized using microscopic techniques. The SEM images showing the cross-section and the surface on the lumen side of SL-TFC membranes are shown in **Figure 4**. Despite that the FO performance of SL-TFC membrane has changed substantially, there was no discernible difference in the morphology of SL-TFC membrane before and after the FO tests, regardless of the concentration of the draw solution used. It implied that the flux decline occurred in SL-

TFC membrane may be caused by microscopic deformations that were too minor to be identified.

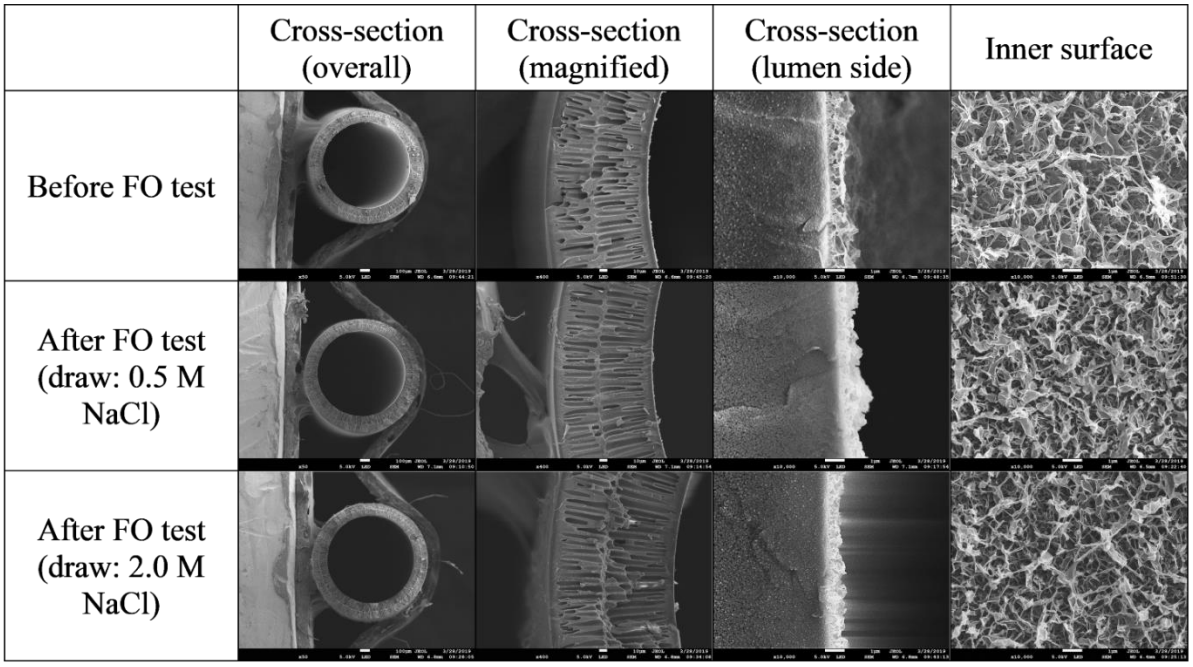

Figure 4. SEM images of SL-TFC membrane before and after FO tests.

Nevertheless, the irreversible changes in the FO performance of SL-TFC membranes with operating time was observed, and the changes were more significant when the draw solution with higher concentration was used. To have a better understanding of these observations, two double-skinned membranes were fabricated and characterized for further investigations.

3.3 FO performance of TFC membrane with dual-layered support (DL#1-TFC)

The DL#1-TFC membrane was fabricated from a hollow fiber substrate with purposely densified skin layer on its shell side. The FO performance of DL#1-TFC membrane was tested for 24 hours, and its water flux, reverse salt flux and specific reverse salt flux are shown in **Figure 5**. For FO test carried out using 0.5 M NaCl as draw solution, the initial water flux, reverse salt flux and specific reverse salt flux of DL#1-TFC membranes were 36.7 L/m^2/h, 5.3 g/m^2/h and 0.15 g/L, respectively; whereas when 2.0 M NaCl was used as draw solution, the initial water flux, reverse salt flux and specific reverse salt flux of DL#1-TFC membranes were 60.1 L/m^2/h, 24.8 g/m^2/h and 0.41 g/L, respectively. The initial specific reverse salt flux of DL#1-TFC membrane was significantly higher when 2.0 M NaCl was used as draw solution,

which may indicate that the selectivity of DL#1-TFC membrane have deteriorated immediately after it was brought into contact with 2.0 M NaCl solution.

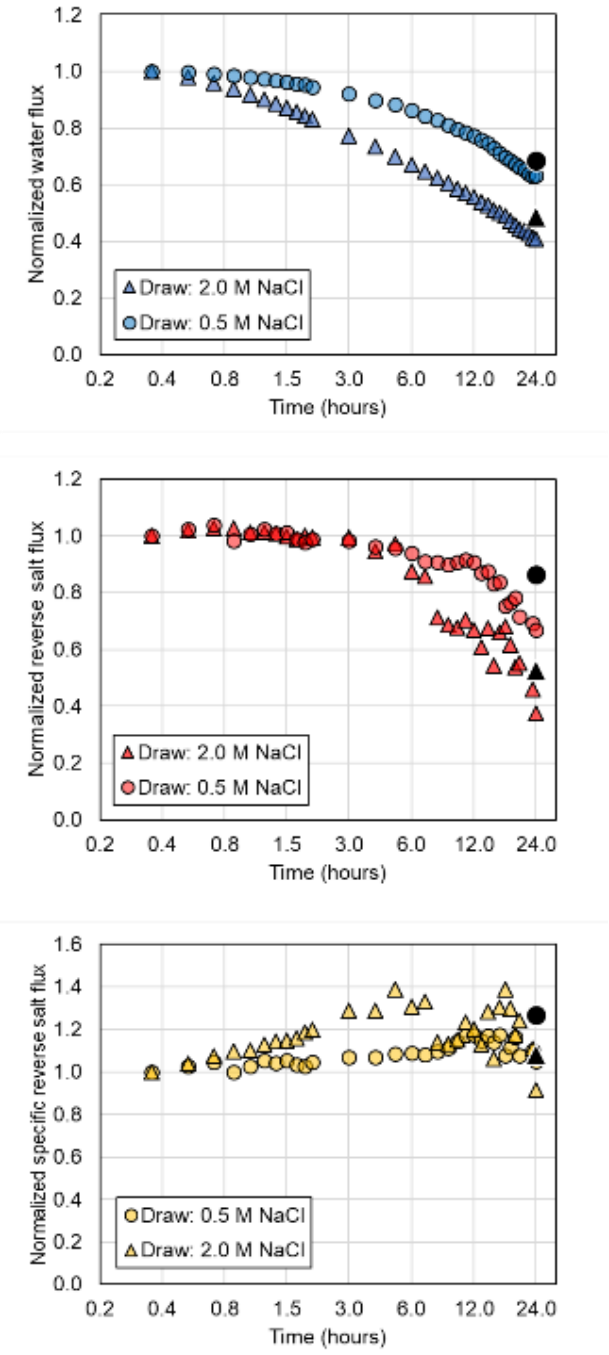

Figure 5. FO performance of DL#1-TFC membrane characterized by using either 0.5 M NaCl or 2.0 M NaCl as draw solution in AL-DS orientation. DI water was used as feed solution. The normalized water flux, normalized reverse salt flux and normalized specific reverse salt flux of the membrane are presented in logarithmic time scale. The final performance of the membrane after 24 hours of experiments are indicated by the bold shaded markers.

When 0.5 M NaCl was used as draw solution, the water flux of DL#1-TFC membrane decreased almost linearly with time starting from the beginning of the FO tests. As the concentration of draw solution was increased to 2.0 M NaCl, the water flux of DL#1-TFC membrane declined even faster with time, which implied that the structure of DL#1-TFC membrane has experienced greater change within a short duration. In addition, the water flux decline during the FO tests appeared to shift towards logarithmic decay pattern when 2.0 M NaCl was used as the draw solution. On the other hand, the DL#1-TFC membrane displayed similar salt flux decline patterns in both FO tests using 0.5 M NaCl and 2.0 NaCl as draw solutions. The reverse salt fluxes appeared to be relatively stable within the first 3 hours, but were found to decrease linearly over time with longer testing duration.

After 24-hour FO tests, the used DL#1-TFC membrane was re-tested using fresh feed and draw solutions. It was found that its water flux decreased by 32% and 52%, whereas the reverse salt flux of the used membrane decreased by 14% and 47% using 0.5 M NaCl and 2.0 M NaCl as the draw solution, respectively, in comparison with the results of fresh DL#1-TFC membrane. Overall, the used DL#1-TFC membrane presented more significant water flux decline and reverse salt flux decline when the draw solution of higher concentration was used in FO tests, similar to the SL-TFC membrane. Yet, the reverse salt flux decline of DL#1-TFC membrane was less significant than water flux decline, which is different from the situation of the SL-TFC membrane. As a result, the specific reverse salt flux increased by 26% and 8% after the FO tests were carried out with 0.5 M NaCl and 2.0 M NaCl as draw solutions. These results implied that the rejection of DL#1-TFC membrane to NaCl has deteriorated during the FO tests..

In order to investigate if the significant deterioration of FO performance was associated with the structural deformation of DL#1-TFC membrane, the membranes were removed from the modules and frozen right after the FO tests, before they were characterized with the microscopic techniques. The cross-section morphology of DL#1-TFC membrane before and after the FO tests were shown in the SEM images in **Figure 6**. It was found that the thickness of the polyamide layer become thinner and the surface was more even. The surface of the polyamide layer surface exhibited loosely bound leafy appearance before FO test, which appeared to become compacted and flattened after FO test. These observations implied that the deterioration of FO performance was likely associated with the microscopic deformation of TFC membrane during the FO tests.

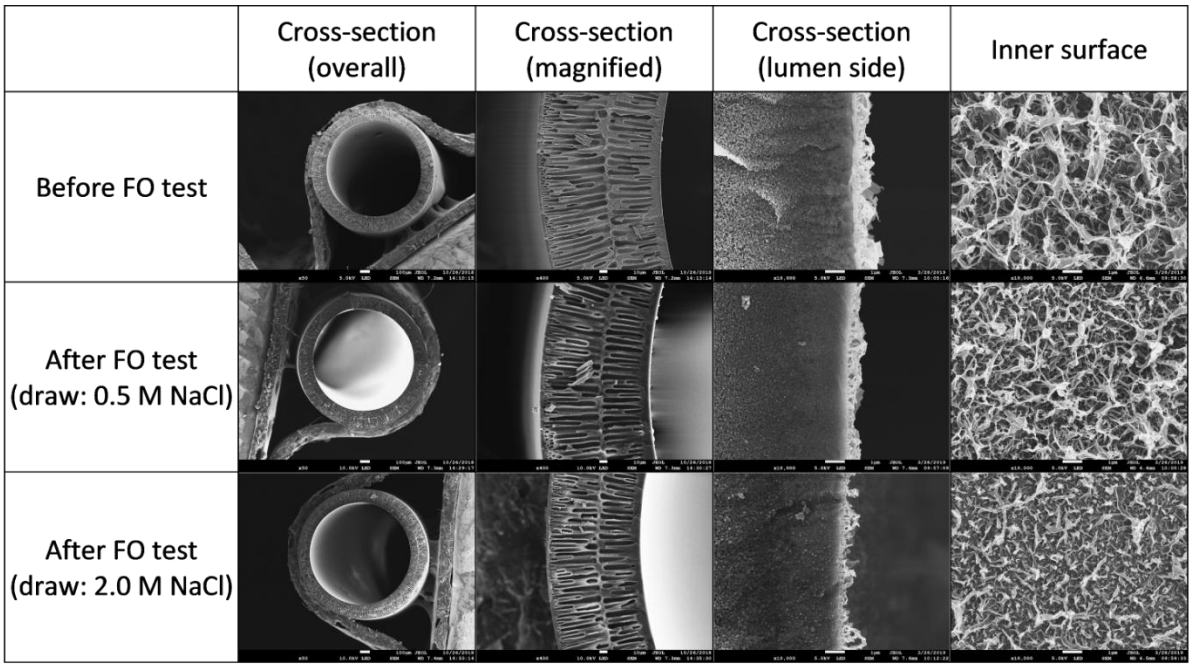

Figure 6. SEM images of DL#1-TFC membrane before and after FO tests.

In comparison with the case of SL-TFC membrane in Section 3.2, both SL-TFC and DL#1-TFC membranes with different support layer structures displayed irreversible decline in water flux and reverse salt flux during FO tests within 24 hours. In addition, the water flux decline of DL#1-TFC membrane was more significant than that of SL-TFC membrane, whose support layer is more permeable than the former. It is also noted that the initial water flux of DL#1-TFC membrane was lower than SL-TFC membrane. Thus, it is speculated that the osmosis-induced compaction of TFC membrane is associated with not only the polyamide layer, but also the support layer structure. A support layer with low permeability may contribute high hydraulic resistance to water permeation and may promote TFC FO membrane's compaction.

3.4 FO performance of TFC membrane with dual-layered support (DL#2-TFC)

To confirm the influence of the hydraulic resistance of support layer on the osmosis-induced compaction, DL#2-TFC membrane was prepared and characterized with the same testing conditions. Similar to DL#1-TFC membrane, DL#2-TFC membrane was prepared from a

hollow fiber substrate that possessed a specially densified skin layer on the shell side. Yet, the water permeability of the substrate of DL#2-TFC membrane was 83% lower than that of DL#1-TFC membrane. Therefore, it was expected that the osmosis-induced compaction would have greater influence on the performance of the DL#2-TFC membrane.

Figure 7 shows the water flux, reverse salt flux and specific reverse salt flux of DL#2-TFC membrane in FO tests. When 0.5 M NaCl was used as the draw solution, the initial water flux, reverse salt flux and specific reverse salt flux of DL#2-TFC membranes were 17.0 L/m^2/h, 7.2 g/m^2/h and 0.42 g/L, respectively. Both water flux and reverse salt flux decreased logarithmically with time, which were similar to the flux patterns observed in the FO performance of DL#1-TFC membrane. On the other hand, the initial water flux, reverse salt flux and specific reverse salt flux of DL#2-TFC membranes were 5.7 L/m^2/h, 6.1 g/m^2/h and 1.02 g/L, respectively, when 2.0 M NaCl was used as the draw solution. It should be noted that the water flux of DL#2-TFC membrane decreased sharply by approximately 75% within the first 5 minutes after the FO test began and stabilized shortly afterwards. Since initial fluxes were determined from the average performance of each membrane at 20 minutes after the FO tests begun, such rapid changes in water flux could not be effectively captured. As such, the subsequent changes presented in Figure 7 may not be reflecting the true behaviour of DL#2-TFC membrane during the FO test when 2.0 M NaCl was used as the draw solution. Meanwhile, the reverse salt flux of DL#2-TFC membrane increased instantly after the FO test began and stabilized shortly after. As a result, the initial specific reverse salt flux of DL#2-TFC membrane using 2.0 M NaCl as draw solution was close to 250% higher than when 0.5 M NaCl was used as draw solution.

These unusual changes in the pattern of water flux and reverse salt flux over time may indicate that a substantial structural deformation occurred almost instantly on DL#2-TFC membrane when it was exposed to a highly concentrated draw solution. It confirmed that the rejection of TFC membrane to NaCl could be seriously compromised due to osmosis-induced compaction when operated over an extremely high osmotic pressure gradient.

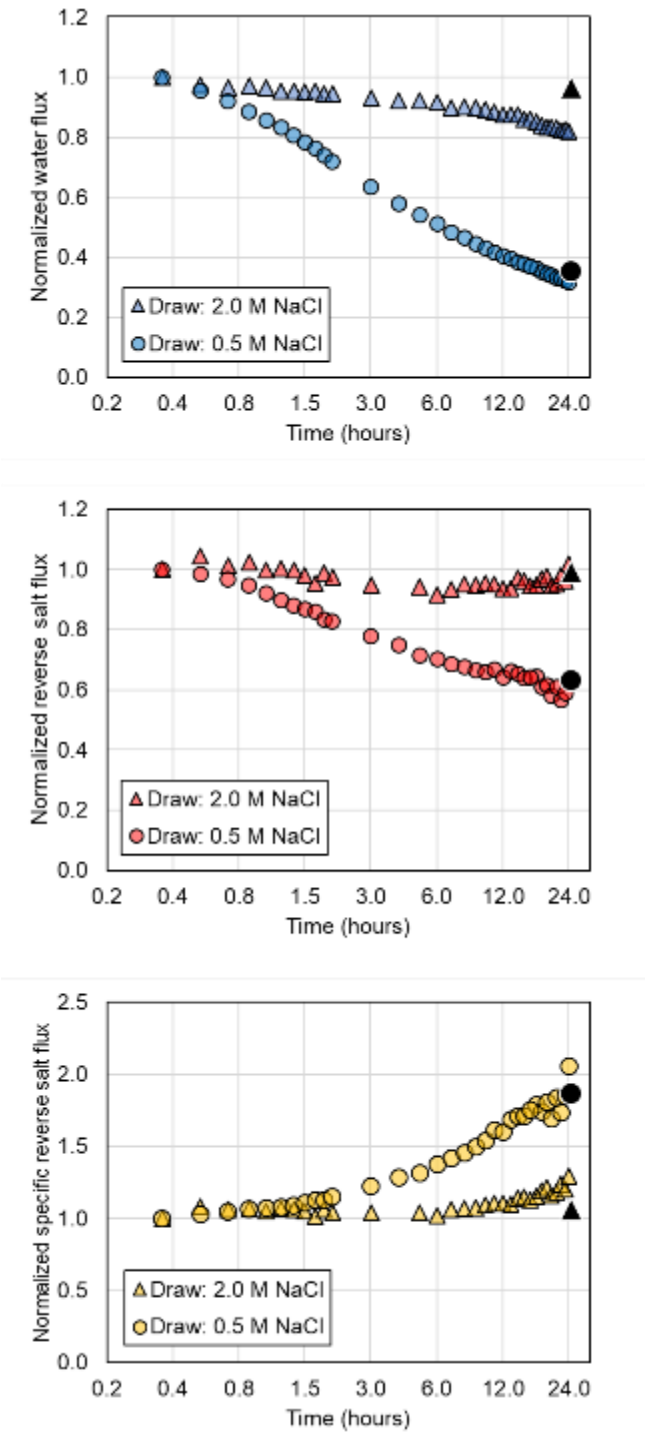

505

506 **Figure 7.** FO performance of DL#2-TFC membrane characterized by using either 0.5 M NaCl
507 or 2.0 M NaCl as draw solution in AL-DS orientation. DI water was used as feed solution. The
508 normalized water flux, normalized reverse salt flux and normalized specific reverse salt flux of
509 the membrane are presented in logarithmic time scale. The final performance of the membrane
510 after 24 hours of experiments are indicated by the bold shaded markers.

511

At the end of FO tests, the water flux of DL#2-TFC decreased by 65% and 4%, while reverse salt flux decreased by 35% and 1%, when 0.5 M NaCl and 2.0 M NaCl fresh draw solutions were used together with fresh feed water, respectively. As expected, the overall water flux reduction and reverse salt flux reduction of DL#2-TFC membrane were significant when 0.5 M NaCl was used as draw solution. It suffered even more significant water flux decline than DL#1-TFC membrane, which confirmed again that osmosis-induced compaction was promoted in TFC membranes that possess a support layer with higher hydraulic resistance.

The cross-section morphology of DL#2-TFC membranes before and after FO tests were observed under SEM, as shown in the images in **Figure 8**. Similar to SL-TFC and DL#1-TFC membranes, the macroscopic morphology of DL#2-TFC membrane was featured by densely packed needle-like macrovoids with bi-layered arrangement, which remained unchanged after the FO tests. However, visible changes in the cross-section morphology can be observed in the regions of the support layer which was lying directly beneath the polyamide selective layer. Before FO tests, the sublayer resembled a highly porous sponge-like structure. After FO tests, the void volume in the sublayer appeared to be lower, and the apparent thickness of polyamide layer also decreased significantly. The changes in the morphology of the sublayer beneath the polyamide layer were more significant after the FO tests with 2.0 M NaCl as draw solution. It was believed that the pore collapse in the sublayer may have contributed significantly to severe reduction in the FO performance of DL#2-TFC membranes.

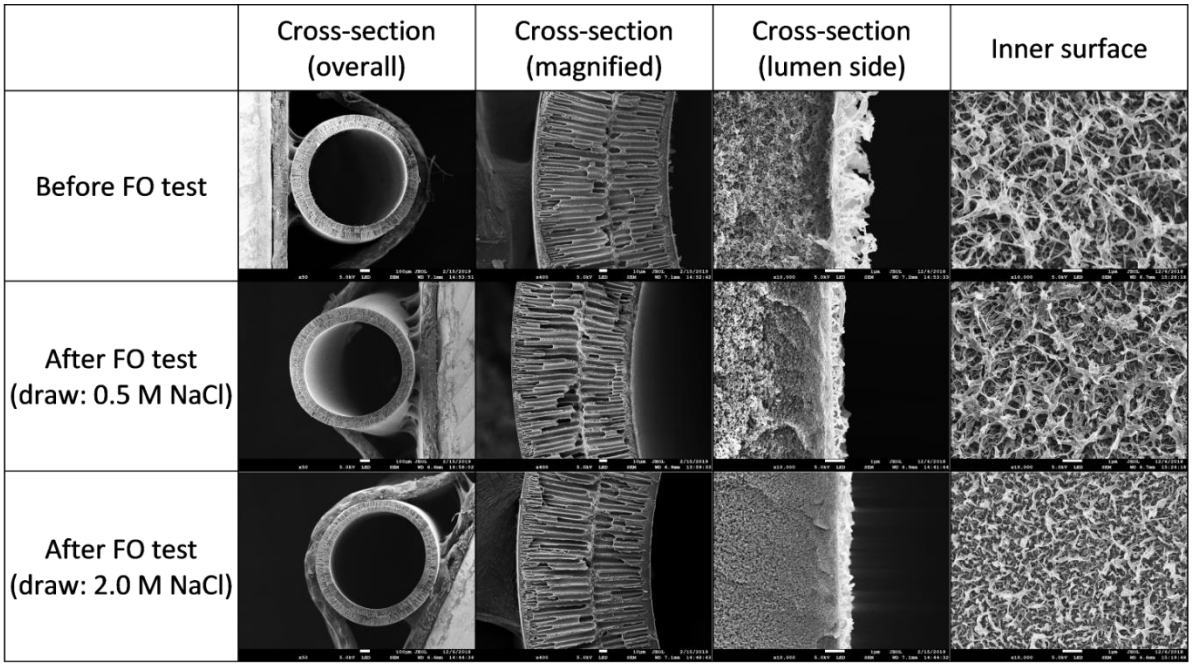

Figure 8. SEM images of DL#2-TFC membrane before and after FO tests.

The effect of osmosis-induced compaction on the structure of the membrane was also evident under TEM. The cross-section morphology of DL#2-TFC membrane near the polyamide layer before and after FO tests are shown in **Figure 9**. Before FO tests, there were some voids in the support layer that were very close to the polyamide layer, and there was no apparent transition in porosity across the section. After FO tests with either 0.5 M NaCl or 2.0 M NaCl as draw solution, the big pores within the support layer disappeared, and a visibly densified band appeared next to the polyamide layer, which confirmed that serious compaction occurred around the skin layers of TFC membrane. These observations confirmed that osmosis-induced compaction could affect the structure of TFC membrane, especially when there was significantly high osmotic pressure difference across the membrane.

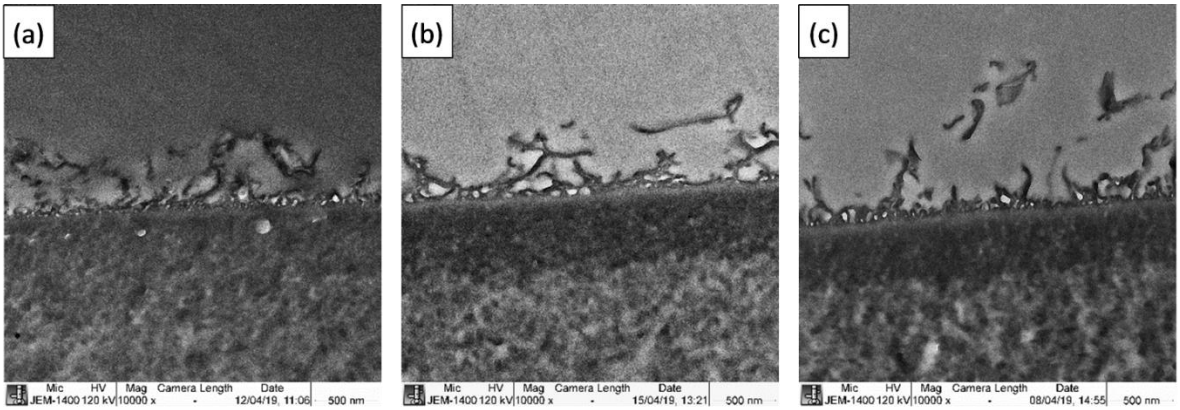

Figure 9. TEM images showing the cross-section morphology of DL#2-TFC membrane near the polyamide selective layer: (a) before FO test, and after 24-hours FO test carried out with either (b) 0.5 M NaCl or (c) 2.0 M NaCl as draw solution.

In addition, the characterization of DL#2-TFC membrane by AFM has revealed that the surface topography of the polyamide layer of the membrane has changed substantially after FO tests. As shown in **Figure 10**, the surface of the polyamide layer before FO test exhibited more spikes-like structures that spread out evenly across membrane surface, which well corresponded to the characteristic ridge-and-valley structures observed under SEM. After FO tests using 0.5 M NaCl as draw solution, some of the protruding structure appeared to have collapsed and the surface became less uniform. After FO tests using 2.0 M NaCl as draw solution, the surface of polyamide layer was apparently flattened, and most of the visible structures observed in the pristine DL#2-TFC membrane were diminished. The average surface roughness (R_a) of the polyamide layer of DL#2-TFC has decreased from 299 nm to 248 nm and 96 nm after FO tests were carried out by using 0.5 M NaCl and 2.0 M NaCl as draw solutions, respectively. The substantial reduction in surface roughness may indicate that there was a substantial pressure difference across the membrane during the FO test, such that the polyamide layer was flattened under the stress exerted.

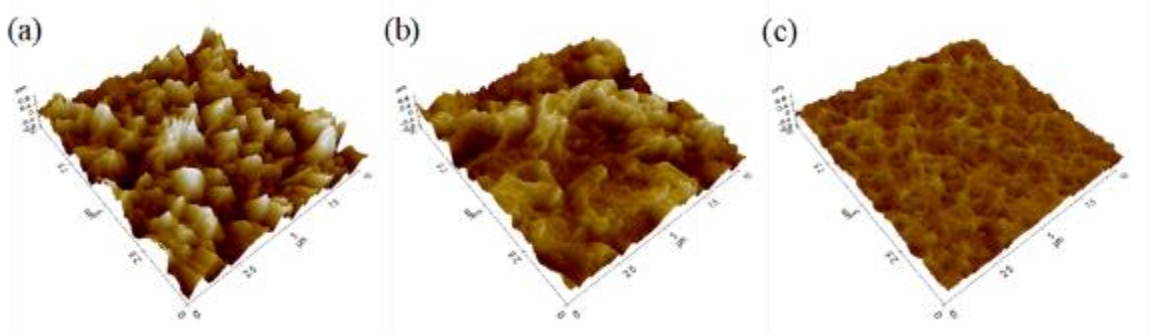

Figure 10. AFM images showing the surface topography of polyamide selective layer of DL#2-TFC membrane (a) before FO test, and after 24-hours FO tests carried out with either (b) 0.5 M NaCl or (c) 2.0 M NaCl as draw solution.

3.5 Mechanism of membrane compaction in forward osmosis process

The collapse of the pore structures beneath the polyamide layer and the smoothening of polyamide layer of DL#2-TFC membrane after FO tests confirmed the membrane compaction in FO process, which should be caused by a substantial mechanical stress imposed on the

membrane though there was no external hydraulic pressure applied on the membrane. In order to understand possible mechanisms behind, the water transport across the membrane and corresponding hydrostatic pressure profile are schematically illustrated in **Figure 11**.

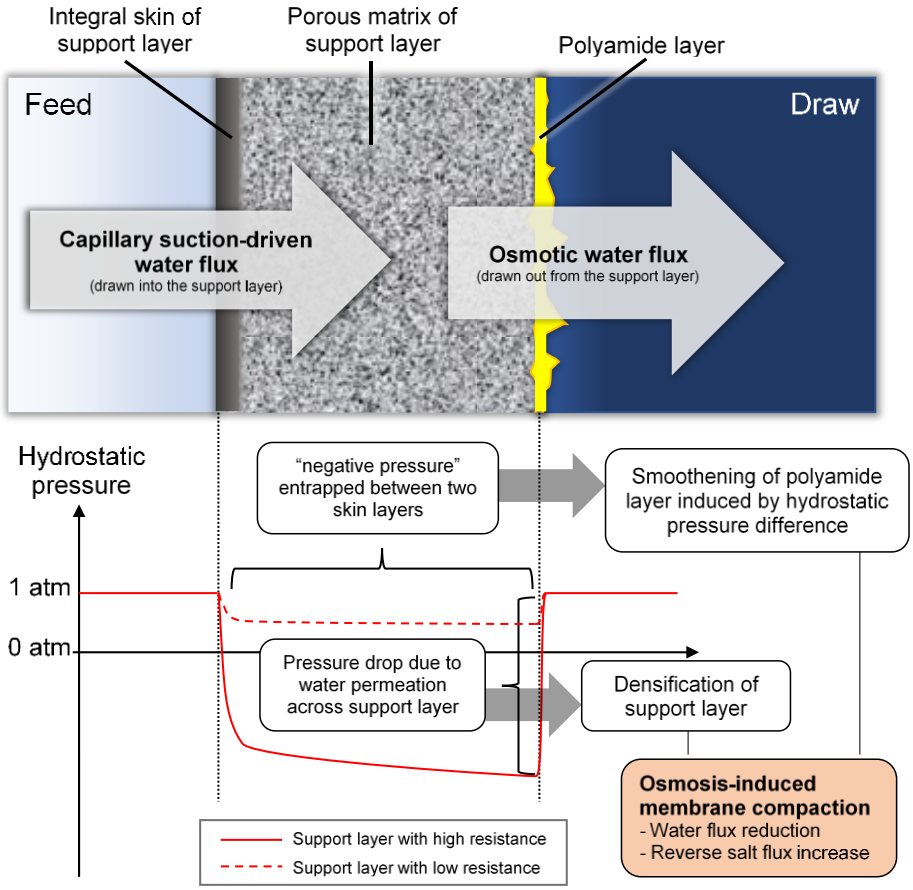

Figure 11. Schematic illustration of osmosis-driven compaction in forward osmosis membrane.

During the FO process, water was drawn across the polyamide selective layer of TFC membrane at a rate proportional to the osmotic pressure difference. Due to the cohesion force of water, water permeation across the support layer should occur at an equal rate as the osmosis-driven water flux to replenish the water lost into the draw solution. As the water permeates through the support layer, the hydraulic resistance of the support layer would induce pressure drop across the support layer which was proportional to the water flux [41]. Thus, there exists a steady-state pressure gradient across the support layer. The local pressure gradient could induce mechanical stress within the support layer, which may cause microscopic deformations of the pore channels such as narrowing and collapse of pores. Eventually, the deformations may obstruct water transport passages within the substrate, which lead to increased hydraulic

586 resistance. As the result, the water flux of the TFC membrane would decrease during FO
587 process when operated in AL-DS orientation.

588 Since SL-TFC membranes possessed porous support layer with high water permeability, the
589 resistance towards water flux through the support layer during FO may be relatively low. As
590 such, when the osmotic water flux is low, the pressure drop across the support layer could be
591 small. It explained the relatively minor water flux decline observed on SL-TFC membrane
592 during FO tests. Nevertheless, the water flux decline of SL-TFC membrane became more
593 significant when it is subjected to FO tests with higher osmotic pressure gradient. It showed
594 that substantial mechanical stress could still occur within TFC membrane that consists of a
595 support layer with high water permeability if the osmotic water flux was sufficiently high. On
596 the other hand, if there is a dense skin layer on the side of the support facing the feed solution,
597 which imposes high hydraulic resistance to the water transport across the support layer, the
598 build-up of the mechanical stress within the TFC membrane could be more severe. The
599 consequence would be more significant water flux decline during FO process, which were
600 clearly observed on DL#1-TFC and DL#2-TFC membranes.

601 On the other hand, since there was no externally applied pressure in FO process, the hydrostatic
602 pressure on both sides of the TFC membrane should be equal at around 1 atm (atmospheric
603 pressure), as depicted in **Figure 11**. However, the hydrostatic pressure within the porous matrix
604 of the support layer could vary significantly, since the lumen side of the support layer is
605 completely segregated from the atmosphere by the polyamide layer. As the result, the pressure
606 drop across the support layer could induce hydrostatic pressure difference across the polyamide
607 layer during FO process. As the polyamide layer was extremely thin, the pressure gradient
608 across the polyamide layer could be substantially higher than that across the support layer.
609 Therefore, a significantly high stress was exerted on the polyamide layer towards the direction
610 facing the support layer. This could explain for the reduction in the thickness of the polyamide
611 layer observed in DL#1-TFC (**Figure 5)** and DL#2-TFC (**Figure 7**) membranes, as well as the
612 smoothening of polyamide layer of DL#2-TFC membrane (**Figure 9**) after the FO tests were
613 carried out. Also, since the polyamide layer rested on the surface of the support layer, the
614 mechanical stress exerted on the polyamide layer was also partly distributed to the support
615 layer, which may cause the deformation of the support layer near the polyamide layer. This
616 was also observed in DL#2-TFC membrane, where visible densification occurred around the
617 region of the support layer in close contact with the polyamide layer (**Figure 8**).

618 The pressure drop across the support layer of TFC membranes could also lead to occurrence of
619 "negative pressure" within the porous matrix of the support layer during FO process, as
620 illustrated in **Figure 11.** In such situation, it is speculated that capillary pressure could maintain
621 the continuity of water flow within the interconnected pores of the support layer. For example,
622 from the SEM images of DL#2-TFC membrane, the diameter the pores within the sponge-like
623 structures near the skin layers on the shell side may be around 0.1 μm or less. This could
624 translate to capillary pressure of approximately 15 bar within the interconnected pores. It is
625 possible that the capillary pressure may suppress the occurrence of vacuum filled cavities
626 within the interconnected pores, as long as the "negative pressure" created by the osmosis-
627 driven water flux across the membrane does not exceed the capillary pressure. The water
628 transport within these double-skinned membranes also closely resembles the water
629 transportation system in plants, where the mechanism of water transport was explained by
630 cohesion-tension theory [42].

631

632 **4. Conclusions**

633 In this study, the deterioration of membrane performance has been observed during FO process
634 in the absence of foulants. The TFC membranes experienced different extents of water flux
635 decline and reverse salt flux decline after FO tests were carried out for 24 hours. It was deduced
636 that the performance of TFC membranes was correlated to the resistance of the support layer
637 of the membrane. As the hydraulic resistance of the support layer increased, the TFC membrane
638 suffered more severe water flux decline than reverse salt flux decline, which led to increasingly
639 more significant decrease in the selectivity of the TFC membranes.

640 The deterioration of FO performance could be largely irreversible, which implied that the TFC
641 membranes might have undergone structure change during the FO tests. The membranes were
642 characterized using SEM, AFM and TEM before and after FO tests, and noticeable changes
643 were observed in the morphology of the cross-section and the surface of the polyamide layer
644 of TFC membrane. The morphology transformation suggested that there was mechanical stress
645 exerting on the TFC membrane during the FO tests. Based on these observations, it was
646 deduced that osmosis-induced compaction was associated with microscopic deformation in the
647 TFC membrane. As the result, the hydraulic resistance of the support layer increased and ICP
648 was aggravated, thus deteriorated the FO performance of TFC membranes.

The current study revealed that the properties of TFC membranes could be significantly affected by membrane compaction during FO process. Compaction of TFC membranes may be caused by build-up of internal stress, which is associated with the hydraulic resistance of the membrane support layer and the rate of water permeation driven by osmosis. The observations also indicated that certain membrane structures (especially double-skinned membranes) may be more susceptible toward osmosis-induced compaction, which could lead to severe deterioration of FO performance. As such, it is suggested that longer testing duration should be applied to ensure that stabilized performance of the FO membranes can be acquired. Also, in analogy to the common practice on pre-compaction of RO membranes under high pressure, if possible, FO membranes may be pre-compacted by operating the membrane with draw solution of higher concentration for a short period of time to accelerate the compaction process and achieve stabilized performance with draw solution of low concentration afterwards.

Acknowledgements

This research grant was supported by the Singapore National Research Foundation under its Urban Solution & Sustainability and administrated by PUB, Singapore's National Water Agency (USS-IF-2018-1). The authors acknowledge Economic Development Board (EDB) of Singapore for funding the Singapore Membrane Technology Centre (SMTC), Nanyang Technological University.

668

669 **References**

670 [1] O.A. Bamaga, A. Yokochi, B. Zabara, A.S. Babaqi, Hybrid FO/RO desalination system: Preliminary
671 assessment of osmotic energy recovery and designs of new FO membrane module configurations,
672 Desalination, 268 (2011) 163-169.
673 [2] M.S. Thabit, A.H. Hawari, M.H. Ammar, S. Zaidi, G. Zaragoza, A. Altaee, Evaluation of forward
674 osmosis as a pretreatment process for multi stage flash seawater desalination, Desalination, 461 (2019)
675 22-29.
676 [3] L. Shi, S.R. Chou, R. Wang, W.X. Fang, C.Y. Tang, A.G. Fane, Effect of substrate structure on the
677 performance of thin-film composite forward osmosis hollow fiber membranes, Journal of Membrane
678 Science, 382 (2011) 116-123.
679 [4] D. Li, Y. Yan, H. Wang, Recent advances in polymer and polymer composite membranes for reverse
680 and forward osmosis processes, Progress in Polymer Science, 61 (2016) 104-155.
681 [5] S. Zou, M. Qin, Z. He, Tackle reverse solute flux in forward osmosis towards sustainable water
682 recovery: reduction and perspectives, Water Research, 149 (2019) 362-374.
683 [6] B. Mi, M. Elimelech, Chemical and physical aspects of organic fouling of forward osmosis
684 membranes, Journal of Membrane Science, 320 (2008) 292-302.
685 [7] Q. She, X. Jin, C.Y. Tang, Osmotic power production from salinity gradient resource by pressure
686 retarded osmosis: Effects of operating conditions and reverse solute diffusion, Journal of Membrane
687 Science, 401-402 (2012) 262-273.
688 [8] Y. Wang, F. Wicaksana, C.Y. Tang, A.G. Fane, Direct Microscopic Observation of Forward Osmosis
689 Membrane Fouling, Environmental Science & Technology, 44 (2010) 7102-7109.
690 [9] D.I. Kim, J. Kim, S. Hong, Changing membrane orientation in pressure retarded osmosis for
691 sustainable power generation with low fouling, Desalination, 389 (2016) 197-206.
692 [10] J. Zhang, W.L.C. Loong, S. Chou, C. Tang, R. Wang, A.G. Fane, Membrane biofouling and scaling in
693 forward osmosis membrane bioreactor, Journal of Membrane Science, 403-404 (2012) 8-14.
694 [11] Q. She, R. Wang, A.G. Fane, C.Y. Tang, Membrane fouling in osmotically driven membrane
695 processes: A review, Journal of Membrane Science, 499 (2016) 201-233.
696 [12] C.Y. Tang, Q. She, W.C.L. Lay, R. Wang, R. Field, A.G. Fane, Modeling double-skinned FO
697 membranes, Desalination, 283 (2011) 178-186.
698 [13] K.Y. Wang, R.C. Ong, T.-S. Chung, Double-Skinned Forward Osmosis Membranes for Reducing
699 Internal Concentration Polarization within the Porous Sublayer, Industrial & Engineering Chemistry
700 Research, 49 (2010) 4824-4831.
701 [14] P.H.H. Duong, T.-S. Chung, S. Wei, L. Irish, Highly Permeable Double-Skinned Forward Osmosis
702 Membranes for Anti-Fouling in the Emulsified Oil–Water Separation Process, Environmental Science
703 & Technology, 48 (2014) 4537-4545.
704 [15] S. Wang, J. Cai, W. Ding, Z. Xu, Z. Wang, Bio-Inspired Aquaporinz Containing Double-Skinned
705 Forward Osmosis Membrane Synthesized through Layer-by-Layer Assembly, Membranes, 5 (2015)
706 369.
707 [16] W. Fang, R. Wang, S. Chou, L. Setiawan, A.G. Fane, Composite forward osmosis hollow fiber
708 membranes: Integration of RO- and NF-like selective layers to enhance membrane properties of anti-
709 scaling and anti-internal concentration polarization, Journal of Membrane Science, 394 (2012) 140-
710 150.
711 [17] W. Fang, C. Liu, L. Shi, R. Wang, Composite forward osmosis hollow fiber membranes: Integration
712 of RO- and NF-like selective layers for enhanced organic fouling resistance, Journal of Membrane
713 Science, 492 (2015) 147-155.

[18] Y.A. Hussain, M.H. Al-Saleh, A viscoelastic-based model for TFC membranes flux reduction during compaction, Desalination, 344 (2014) 362-370.
[19] V.E. Reinsch, A.R. Greenberg, S.S. Kelley, R. Peterson, L.J. Bond, A new technique for the simultaneous, real-time measurement of membrane compaction and performance during exposure to high-pressure gas, Journal of Membrane Science, 171 (2000) 217-228.
[20] M.T.M. Pendergast, J.M. Nygaard, A.K. Ghosh, E.M.V. Hoek, Using nanocomposite materials technology to understand and control reverse osmosis membrane compaction, Desalination, 261 (2010) 255-263.
[21] S. Zhao, Z. Wang, X. Wei, B. Zhao, J. Wang, S. Yang, S. Wang, Performance Improvement of Polysulfone Ultrafiltration Membrane Using Well-Dispersed Polyaniline–Poly(vinylpyrrolidone) Nanocomposite as the Additive, Industrial & Engineering Chemistry Research, 51 (2012) 4661-4672.
[22] H. Mehdizadeh, J.M. Dickson, P.K. Eriksson, Temperature effects on the performance of thin-film composite, aromatic polyamide membranes, Industrial & Engineering Chemistry Research, 28 (1989) 814-824.
[23] W.C.M. Henkens, J.A.M. Smit, Salt rejection and flux in reverse osmosis with compactible membranes, Desalination, 28 (1979) 65-85.
[24] D.A. Ladner, A. Subramani, M. Kumar, S.S. Adham, M.M. Clark, Bench-scale evaluation of seawater desalination by reverse osmosis, Desalination, 250 (2010) 490-499.
[25] M. Aghajani, M. Wang, L.M. Cox, J.P. Killgore, A.R. Greenberg, Y. Ding, Influence of support-layer deformation on the intrinsic resistance of thin film composite membranes, Journal of Membrane Science, 567 (2018) 49-57.
[26] B.W. Rowe, B.D. Freeman, D.R. Paul, Physical aging of ultrathin glassy polymer films tracked by gas permeability, Polymer, 50 (2009) 5565-5575.
[27] T.M. Murphy, B.D. Freeman, D.R. Paul, Physical aging of polystyrene films tracked by gas permeability, Polymer, 54 (2013) 873-880.
[28] N. Müller, U.A. Handge, V. Abetz, Physical ageing and lifetime prediction of polymer membranes for gas separation processes, Journal of Membrane Science, 516 (2016) 33-46.
[29] U.A. Handge, Analysis of compaction and life-time prediction of porous polymer membranes: influence of morphology, diffusion and creep behaviour, Polymer International, 66 (2017) 521-531.
[30] Y. Kurokawa, M. Kurashige, N. Yui, A viscoelastic model for initial flux decline through reverse osmosis membrane, Desalination, 52 (1984) 9-14.
[31] J.M. Arsuaga, M.J. López-Muñoz, J. Aguado, A. Sotto, Temperature, pH and concentration effects on retention and transport of organic pollutants across thin-film composite nanofiltration membranes, Desalination, 221 (2008) 253-258.
[32] C.Y. Tang, Y.-N. Kwon, J.O. Leckie, Effect of membrane chemistry and coating layer on physiochemical properties of thin film composite polyamide RO and NF membranes: I. FTIR and XPS characterization of polyamide and coating layer chemistry, Desalination, 242 (2009) 149-167.
[33] J.R. McCutcheon, R.L. McGinnis, M. Elimelech, A novel ammonia—carbon dioxide forward (direct) osmosis desalination process, Desalination, 174 (2005) 1-11.
[34] N.Y. Yip, A. Tiraferri, W.A. Phillip, J.D. Schiffman, M. Elimelech, High Performance Thin-Film Composite Forward Osmosis Membrane, Environmental Science & Technology, 44 (2010) 3812-3818.
[35] D.Y.F. Ng, B. Wu, Y. Chen, Z. Dong, R. Wang, A novel thin film composite hollow fiber osmotic membrane with one-step prepared dual-layer substrate for sludge thickening, Journal of Membrane Science, 575 (2019) 98-108.
[36] R. Wang, L. Shi, C.Y. Tang, S. Chou, C. Qiu, A.G. Fane, Characterization of novel forward osmosis hollow fiber membranes, Journal of Membrane Science, 355 (2010) 158-167.
[37] L. Setiawan, R. Wang, L. Shi, K. Li, A.G. Fane, Novel dual-layer hollow fiber membranes applied for forward osmosis process, Journal of Membrane Science, 421 (2012) 238-246.
[38] Z.L. Cheng, X. Li, Y.D. Liu, T.-S. Chung, Robust outer-selective thin-film composite polyethersulfone hollow fiber membranes with low reverse salt flux for renewable salinity-gradient energy generation, Journal of Membrane Science, 506 (2016) 119-129.

765 [39] S. Singh, K.C. Khulbe, T. Matsuura, P. Ramamurthy, Membrane characterization by solute
766 transport and atomic force microscopy, Journal of Membrane Science, 142 (1998) 111-127.
767 [40] C.Y. Tang, Y.-N. Kwon, J.O. Leckie, Probing the nano- and micro-scales of reverse osmosis
768 membranes—A comprehensive characterization of physiochemical properties of uncoated and coated
769 membranes by XPS, TEM, ATR-FTIR, and streaming potential measurements, Journal of Membrane
770 Science, 287 (2007) 146-156.
771 [41] E. Di Giuseppe, M. Moroni, M. Caputo, Flux in Porous Media with Memory: Models and
772 Experiments, Transport in Porous Media, 83 (2010) 479-500.
773 [42] E. Steudle, THE COHESION-TENSION MECHANISM AND THE ACQUISITION OF WATER BY PLANT
774 ROOTS, Annual Review of Plant Physiology and Plant Molecular Biology, 52 (2001) 847-875.

775